ATLAS NOTE

ATLAS-CONF-2011-098

July 20, 2011

Search for supersymmetry in pp collisions at $\sqrt{s} = 7$ TeV in final states with missing transverse momentum, b-jets and no leptons with the ATLAS detector

ATLAS Collaboration

ATLAS-CONF-2011-098
21 July 2011

Abstract

A search for supersymmetric particles in events with large missing transverse momentum, heavy flavour jet candidates and no leptons (e,μ) in $\sqrt{s} = 7$ TeV proton-proton collisions is presented. In a data sample corresponding to an integrated luminosity of 0.83 fb^{-1} recorded by the ATLAS experiment at the Large Hadron Collider, no significant excess is observed with respect to the prediction for Standard Model processes. For R-parity conserving models in which sbottoms are the only squarks to appear in the gluino decay cascade, gluino masses below 720 GeV are excluded at the 95% C.L. Model-independent cross section upper limits are provided in the context of simplified models and the result is also interpreted in the context of grand unification SO(10) models.

1 Introduction

Supersymmetry (SUSY) [1] is one of the most compelling theories to describe physics beyond the Standard Model (SM). In the framework of a generic R-parity conserving minimal supersymmetric extension of the SM, the MSSM [2], SUSY particles are produced in pairs and the lightest supersymmetric particle (LSP) is stable. In a large variety of models, the LSP is the lightest neutralino, $\tilde{\chi}_1^0$, which is weakly interacting and is a possible candidate for dark matter. The coloured superpartners of quarks and gluons, the squarks ($\tilde{q}$) and gluinos ($\tilde{g}$), are expected to be copiously produced via the strong interaction at the Large Hadron Collider (LHC). The partners of the right-handed and left-handed quarks, $\tilde{q}_R$ and $\tilde{q}_L$, can mix to form two mass eigenstates. These mixing effects are proportional to the corresponding fermion masses and therefore become important for the third generation. In particular, large mixing can yield sbottom ($\tilde{b}_1$) and stop ($\tilde{t}_1$) mass eigenstates that are significantly lighter than other squarks. Consequently, $\tilde{b}_1$ and $\tilde{t}_1$ could be produced with large cross sections at the LHC, either via direct pair production or, if kinematically allowed, through $\tilde{g}\tilde{g}$ production with subsequent $\tilde{g} \to \tilde{b}_1 b$ or $\tilde{g} \to \tilde{t}_1 t$ decays. Depending on the SUSY particle mass spectrum, the cascade decays of gluino-mediated and pair-produced sbottoms or stops result in complex final states consisting of missing transverse momentum[1] and several jets, among which b-quark jets (b-jets) are expected. First searches for the production of SUSY particles in b-jets enriched final states at the LHC have been published recently [3, 4]. In this note an update of the search in Ref. [3] is presented.

SUSY is searched for in final states involving $E_{\mathrm{T}}^{\mathrm{miss}}$, energetic jets, of which at least one must be identified as a b-jet and no isolated leptons (e or μ). The search is based on pp collision data at a centre-of-mass energy of 7 TeV recorded by the ATLAS experiment [5] at the LHC in 2011. The total data set included in the analysis corresponds to an integrated luminosity of 0.83 fb^{-1}.

Two phenomenological MSSM scenarios are considered where the first and second generation squark masses are set above 2 TeV. In the first scenario, the $\tilde{b}_1$ is the lightest squark and $m_{\tilde{g}} > m_{\tilde{b}_1} > m_{\tilde{\chi}_1^0}$ and the branching ratio for $\tilde{g} \to \tilde{b}_1 b$ decays is 100%. Sbottoms are produced via gluino-mediated processes or via direct pair production and they are assumed to decay exclusively via $\tilde{b}_1 \to b\tilde{\chi}_1^0$, where $m_{\tilde{\chi}_1^0}$ is fixed at 60 GeV to escape bounds from direct searches. The interpretation of the results is presented as a function of the gluino and light sbottom masses. The second MSSM-like scenario is defined in the context of the general simplified models [6]: all squarks including $\tilde{b}_1$ are heavy, gluino-pair production is the only kinematically allowed process and gluinos decay (off-shell) into $b\bar{b}\tilde{\chi}_1^0$ final states. Here the results are interpreted in a $(m_{\tilde{g}}, m_{\tilde{\chi}_1^0})$ plane. The results are also generalised to any new physics process where gluino-like particles decay into $b\bar{b}$ and a weakly interacting massive particle.

Finally the results are interpreted in the context of specific Grand Unification Theories (GUTs) based on the gauge group SO(10) [7]. In this scenario, the SUSY particle mass spectrum is characterised by low masses of the gluinos (300-600 GeV), charginos (100-180 GeV) and neutralinos (50-90 GeV), with $m_{\tilde{\chi}_2^0} \approx 2 \times m_{\tilde{\chi}_1^0}$. First and second generation scalars have masses of about 10 TeV whereas third generation squarks, Higgs scalars and μ are of the order of 1-3 TeV. Depending on the sparticle masses, chargino-neutralino and gluino-pair production dominate. The three-body gluino decays $\tilde{g} \to b\bar{b}\tilde{\chi}_1^0$ and $\tilde{g} \to b\bar{b}\tilde{\chi}_2^0$ are expected to lead to final states with high b-jet multiplicities. Two specific models are considered [8], the D-term splitting model, DR3, and the Higgs splitting model, HS.

[1] Its magnitude is referred to as $E_{\mathrm{T}}^{\mathrm{miss}}$ in the following.

Physics process	$\sigma \cdot$ BR [nb]	
$W \to \ell\nu$ (+jets)	31.4±1.6	[14–16]
$Z/\gamma^* \to \ell\ell$ (+jets)	3.20±0.16	[14–16]
$Z \to \nu\nu$ (+jets)	5.82±0.29	[14–16]
$t\bar{t}$	$0.165^{+0.011}_{-0.016}$	[17–19]
Single top	0.085±0.003	[20,21]

Table 1: The most important background processes and their predicted cross sections, multiplied by the relevant branching ratios (BR) before any event selection. A generator level cut $m_{\ell\ell} > 40$ GeV was applied to the $Z/\gamma^*(\to \ell^+\ell^-)$ process. Contributions from higher order QCD corrections are included for W and Z boson production (NNLO corrections) and for $t\bar{t}$ production (NLO+NNLL corrections).

2 Monte Carlo simulated samples

Simulated event samples are used to determine the detector acceptance, the reconstruction efficiencies and the expected event yields for signal and background processes.

Samples of SUSY signal processes were simulated for various models using the HERWIG++ [9] v2.4.2 Monte Carlo program. The particle mass spectra and decay modes were determined using the ISASUSY package from the ISAJET [10] v7.80 and the SUSYHIT [11] v1.3 programs. The latter was used for the MSSM scenarios, which are parametrised in the $(m_{\tilde{g}}, m_{\tilde{b}_1})$ and $(m_{\tilde{g}}, m_{\tilde{t}_1})$ planes, with gluino masses above 300 GeV. The SUSY sample yields are then normalised to the expectations from next-to-leading order (NLO) calculations obtained using the PROSPINO [12] v2.1 program. For these calculations the CTEQ6.6M [13] parametrisation of the parton density functions (PDFs) is used and the renormalisation and factorisation scales are set to the average mass of the sparticles produced in the hard interaction.

For the background, the following Standard Model processes are considered:

- $t\bar{t}$ and single top production: events were generated using the generator MC@NLO [22,23] v3.41. For the evaluation of systematic uncertainties, additional $t\bar{t}$ samples were generated using the POWHEG [24], ALPGEN [25] and ACERMC [26] programs.

- $W(\to \ell\nu)$+jets, $Z/\gamma^*(\to \ell^+\ell^-)$+jets (where $\ell = e,\ \mu,\ \tau$) and $Z(\to \nu\bar{\nu})$ +jets production: events with light and heavy (b,c) flavour jets were generated using the ALPGEN v2.13 program. A generator level cut $m_{\ell\ell} > 40$ GeV was applied to the $Z/\gamma^*(\to \ell^+\ell^-)$ process.

- Di-boson (WW, WZ and ZZ) production: events were generated using ALPGEN, however, compared to the other backgrounds their contribution was found to be negligible, after the application of the selection criteria.

For the QCD background, no reliable prediction can be obtained from a leading order Monte Carlo simulation and a data-driven method is used to determine the contribution to the selected event samples, as discussed in Section 4.

All signal and background samples were generated at $\sqrt{s} = 7$ TeV using the ATLAS MC10 parameter tune [27], processed with the GEANT4 [28] simulation of the ATLAS detector [29], then reconstructed and passed through the same analysis chain as the data. For all generators, except for PYTHIA, the HERWIG + JIMMY [9,30] modelling of the parton shower and underlying event was used (v6.510 and v4.31, respectively).

For the comparison to data, all non-QCD background cross sections are normalised to the results of higher order QCD calculations. A summary of the relevant cross sections is given in Table 1. For the next-to-next-to-leading order (NNLO) W and Z/γ^* production cross sections, an uncertainty of $\pm 5\%$ is assumed. For the $t\bar{t}$ production cross section, the corresponding uncertainty on the NLO+NNLL (next-to-next-to-leading logarithms) cross section is estimated to be $^{+6.5\%}_{-9.5\%}$.

All Monte Carlo samples are generated with both in-time and out-of-time pile-up from multiple proton–proton interactions. The simulated events are reweighted such that the distribution of interactions per crossing in the Monte Carlo matches the one observed in data.

3 Data and Event Selection

After the application of beam, detector and data-quality requirements, the data set used for this analysis correspond to a total integrated luminosity of 0.83 fb^{-1}.

Events are selected at the trigger level by requiring one jet with high p_{T} and large missing transverse momentum. The selection is fully efficient for events containing at least one jet with $p_{\mathrm{T}} > 130$ GeV and $E_{\mathrm{T}}^{\mathrm{miss}} > 130$ GeV [31].

In the data sample selected, jet candidates are reconstructed using the anti-k_t jet clustering algorithm [32–34] with a distance parameter of R=0.4. The inputs to this algorithm are three dimensional calorimeter energy clusters. The reconstructed jet energies are corrected for inhomogeneities and for the non-compensating nature of the calorimeter by using p_{T}- and η-dependent calibration factors determined from Monte Carlo simulation and validated using extensive test-beam measurements and studies of pp collision data (Ref. [35] and references therein). Only jets with $p_{\mathrm{T}} > 20$ GeV and within $|\eta| < 2.8$ are retained for this analysis. Candidates for b-jets are identified among jets with $p_{\mathrm{T}} > 50$ GeV using an algorithm that reconstructs a vertex from all tracks which are displaced from the primary vertex and associated with the jet. The parameters of the algorithm are chosen such that a tagging efficiency of 50% (1%) is achieved for b-jets (light flavour or gluon jets) in $t\bar{t}$ events in Monte Carlo simulation [36].

In order to apply the lepton veto, electron candidates are required to satisfy the 'medium' selection criteria, as detailed in Ref. [37]. Muon candidates are identified either as a match between an extrapolated inner detector track and one or more segments in the muon spectrometer, or by associating an inner detector track to a muon spectrometer track. The combined track parameters are derived from a statistical combination of the two sets of track parameters. Electrons (muons) are required to have $p_{\mathrm{T}} > 20$ GeV (10 GeV) and $|\eta| < 2.47(2.4)$.

The calculation of $E_{\mathrm{T}}^{\mathrm{miss}}$ is based on the modulus of the vectorial sum of the p_{T} of the reconstructed jets (with $p_{\mathrm{T}} > 20$ GeV and over the full calorimeter coverage $|\eta| < 4.9$), leptons (including non–isolated muons) and the calorimeter clusters not belonging to reconstructed objects.

After object identification, overlaps are resolved. Any jet within a distance ΔR = 0.2 of a medium electron candidate is discarded and any remaining lepton within $\Delta R = 0.4$ of a jet is discarded.

Events are selected if the primary vertex is associated with five or more tracks. They are also required to pass basic quality criteria to discriminate against detector noise and non-collision backgrounds. Due to a front–end electronics failure in one of the electromagnetic calorimeter modules, a region of the calorimeter of size $\Delta\eta \times \Delta\phi = 1.6 \times 0.4$ was only partially read out. Events with any jet with $p_{\mathrm{T}} > 50$ GeV in this region are rejected. The acceptance loss caused by this selection cut is about 10%.

Selected events are required to have at least one jet with $p_T > 130$ GeV, at least two additional jets with $p_T > 50$ GeV and $E_T^{miss} > 130$ GeV. At least one jet is required to be b-tagged. Events containing electron or muon candidates are rejected. The effective mass, m_{eff}, is defined as the scalar sum of E_T^{miss} and the transverse momenta of the three leading jets. Events are required to have $E_T^{miss}/m_{eff} > 0.25$. In addition, the smallest azimuthal separation between the E_T^{miss} direction and the three leading jets, $\Delta\phi_{min}$, is required to be larger than 0.4. The last requirement effectively reduces the amount of QCD background where E_T^{miss} results from misreconstructed jets or from neutrinos emitted along the direction of the jet axis by heavy flavour decays.

Four signal regions are defined in order to obtain good signal sensitivity for the various models and parameter values studied. They are characterised by the minimum number of b-jets required in the final state and by the threshold of the further selection on m_{eff}: 3JA ($\geq$1 b-jet, $m_{eff} > 500$ GeV), 3JB ($\geq$1 b-jet, $m_{eff} > 700$ GeV), 3JC ($\geq$2 b-jet, $m_{eff} > 500$ GeV) and 3JD ($\geq$2 b-jet, $m_{eff} > 700$ GeV).

4 Standard Model Background Estimation

The expected amount of $t\bar{t}$, W/Z+jets and single top events is estimated using the Monte Carlo simulation. Events from $t\bar{t}$ production represent the largest background component in all four signal regions. The Monte Carlo prediction is validated by a data-driven estimate which relies on control regions with the same kinematic selection on jets and missing transverse momentum and an electron or a muon with $p_T > 20$ GeV in the final state, $m_{eff} > 600$ GeV and 40 GeV$< m_T <$100 GeV (where m_T is the transverse mass computed from the lepton 4-vector and the E_T^{miss}) and at least one or two b-jets. The normalisation determined in these control regions (corrected for non-$t\bar{t}$ contamination) is then transferred to the kinematically similar signal regions. Figure 1 shows the m_{eff} distribution in the 1-electron and 1-muon (1 b-tag) control regions. The agreement between the data and the Monte Carlo prediction is good and, as a consequence, the prediction of the data-driven estimation agrees with that of the Monte Carlo.

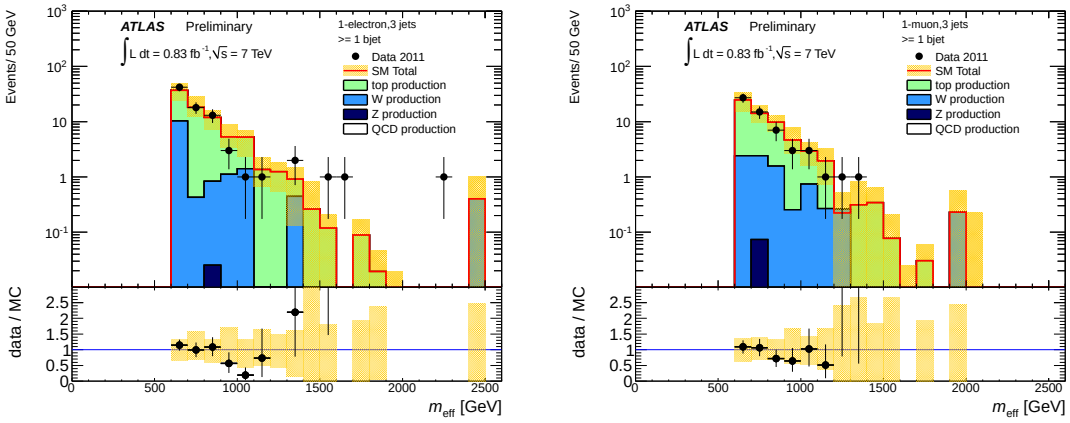

Figure 1: Effective mass distribution for the 1-electron (left) and 1-muon (right) $t\bar{t}$ control regions. The lower plot shows the bin-by-bin ratio of the data to the MC. The yellow band shows the full systematic uncertainty on the SM expectation.

The Monte Carlo estimation of the W/Z background, which is done using ALPGEN as base-

line generator, includes a dedicated simulation of $W+$ heavy flavour quarks. Double counting arising both at generator and at Matrix Element/Parton Shower matching level between samples generated with light and heavy flavour quarks is resolved using a ΔR matching between partons and jets and a dedicated overall normalisation scale factor is applied to the $W+$ heavy flavour samples. For each signal region, the normalisation of the inclusive W/Z Monte Carlo prediction is validated with a combined fit of $t\bar{t}$ and W/Z background components to the distribution of the number of b-tagged jets in a 0-lepton control region defined by reverting the m_{eff} cut. The fit confirms the Monte Carlo prediction.

Since its contribution to the total background is small, the estimation for the single top background is based entirely on the Monte Carlo prediction.

The remaining QCD background in the signal regions is estimated with a data driven procedure. The technique [38, 39] used is to smear the momentum of jets in clean data events with low $E_{\text{T}}^{\text{miss}}$ to generate "pseudoevents" with possibly large $E_{\text{T}}^{\text{miss}}$ values. The method was validated by comparing data and pseudoevents distributions in QCD enriched control regions that are kinematically similar to the signal regions, obtained by reverting the cut on $\Delta\phi_{min}$. Figure 2 shows the m_{eff} distribution for events with $\Delta\phi_{min} < 0.4$ and 1 (left) or 2 (right) b-tagged jets. The emulated QCD distributions agree with the data.

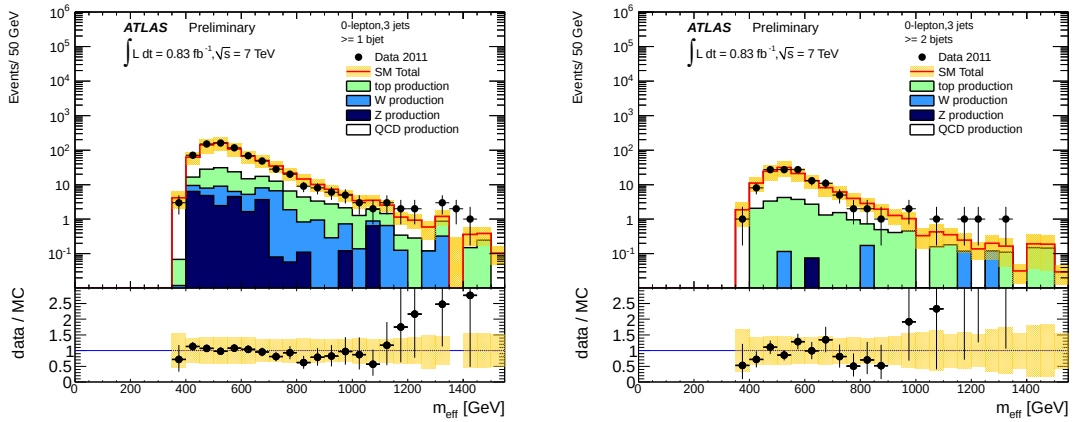

Figure 2: Effective mass distribution for the QCD control region ($\Delta\phi_{min} < 0.4$) for events with 1 (left) or 2 (right) b-tagged jets. The lower plot shows the bin-by-bin ratio of the data to the SM expectation. The QCD prediction validated in these control samples is derived using the smearing method described in the text, other SM background contributions are estimated from MC. The yellow band shows the full systematic uncertainty on the SM expectation

5 Systematic Uncertainties

The background from top and W/Z production is obtained using the Monte Carlo simulation. The total uncertainty on this prediction is estimated to be between $\pm 30\%$ and $\pm 35\%$ depending on the final selection. It is dominated by the uncertainty on the jet energy scale, on the theoretical prediction of the background processes and on the determination of the b-tagging efficiency. The uncertainty on the jet energy scale (derived using 2010 collision data [35]) varies as a function of the jet p_{T} and pseudorapidity and it is about 2% at $p_{\text{T}} = 50$ GeV in the central detector region. Additional systematic uncertainties arise from the dependence of the jet response on

the number of expected interactions per bunch crossing and on the jet flavour. The total jet energy scale uncertainty at 50 GeV in the central detector region is about 5%. This translates into a 20–25% uncertainty on the absolute prediction of the background from SM processes. Uncertainties on the theoretical cross sections of the background processes (see Section 2), on the modelling of initial and final-state soft gluon radiation and the limited knowledge of the PDFs of the proton lead to uncertainties of $\pm 25\%$ and $\pm 30\%$ on the absolute predictions of the $t\bar{t}$ and the W/Z+jet backgrounds, respectively. An additional uncertainty of 50%(100%) is assigned to the associated production of $W(Z)$ and heavy flavour jets. The uncertainty on the determination of the tagging efficiency for b-jets, c-jets and light flavour jets introduces further uncertainties on the predicted background contributions at the level of $\pm 10\%$ ($\pm 22\%$) for $t\bar{t}$ and $\pm 15\%$ ($\pm 30\%$) for W/Z+jets in the 1 (2) b-tag signal regions. For the QCD background estimation, the uncertainty of 50% is dominated by the dependency of the smearing function on the flavour composition of the low $E_{\mathrm{T}}^{\mathrm{miss}}$ sample used as smearing starting point.

For the SUSY signal processes, various sources of uncertainties affect the theoretical NLO cross sections. Variations of the renormalisation and factorisation scales by a factor of two result in uncertainties of $\pm 16\%$ for $\tilde{g}\tilde{g}$ production and $\pm 30\%$ for $\tilde{b}_1\tilde{b}_1$ pair production, with little dependence on the sparticle masses and the SUSY model.

The number of predicted signal events is also affected by the PDF uncertainties, estimated using the CTEQ6.6M PDF error eigenvector sets at the 90% C.L. limit, rescaled to 1σ. The relative uncertainties on the $\tilde{g}\tilde{g}$ ($\tilde{b}_1\tilde{b}_1$) cross sections were estimated to be in the range from $\pm 11\%$ to $\pm 25\%$ ($\pm 7\%$ to $\pm 16\%$) for the $\tilde{g}\tilde{g}$ ($\tilde{b}_1\tilde{b}_1$) processes, depending on the gluino and sbottom masses. Uncertainties due to the modelling of initial and final state radiation on the signal are not included.

The impact of detector-related uncertainties, such as the jet energy scale (JES) and b-tagging uncertainties, on the signal event yields depends on the masses of the produced sparticles. The total uncertainty varies between $\pm 20\%$ ($\pm 35\%$) and $\pm 10\%$ ($\pm 10\%$) for the 1 (2) b-tag case as the gluino/sbottom masses increase from 200 GeV to 1 TeV, across the different scenarios, and it is dominated by the JES and the b-tagging uncertainty for low and high mass sparticles, respectively.

Finally, an additional $\pm 4.5\%$ uncertainty on the quoted total integrated luminosity was taken into account, based on the 2010 luminosity calibration [40] which was transferred to the 2011 data by using the LAr forward calorimeter and the tile calorimeter current measurements.

6 Results

A good agreement between data and Monte Carlo prediction is observed in the distributions of the $\mathrm{m_{eff}}$, the $E_{\mathrm{T}}^{\mathrm{miss}}$ and the p_{T} of the leading jet as shown in Figure 3 before the $\mathrm{m_{eff}}$ cut for the signal regions with one and two b-tags.

The observed and predicted event yields in the four signal regions are given in Table 2 together with the total estimated uncertainty on the predictions. The value used for the top background estimate includes the $t\bar{t}$ and the single top contributions as predicted by the Monte Carlo. The $t\bar{t}$ component is validated using a dedicated data driven procedure. The W/Z+jets background is estimated using Monte Carlo, and the uncertainties correspond to those discussed in Section 5. QCD-multijet contributions are estimated with the jet smearing method. The SM predictions agree with the observed number of events in all four signal regions. For illustration, the distributions of one reference SUSY signal scenario with gluino mass of 700 GeV and sbottom mass of 380 GeV are superimposed.

Since no excess with respect to the SM predictions is observed in the data, the results are

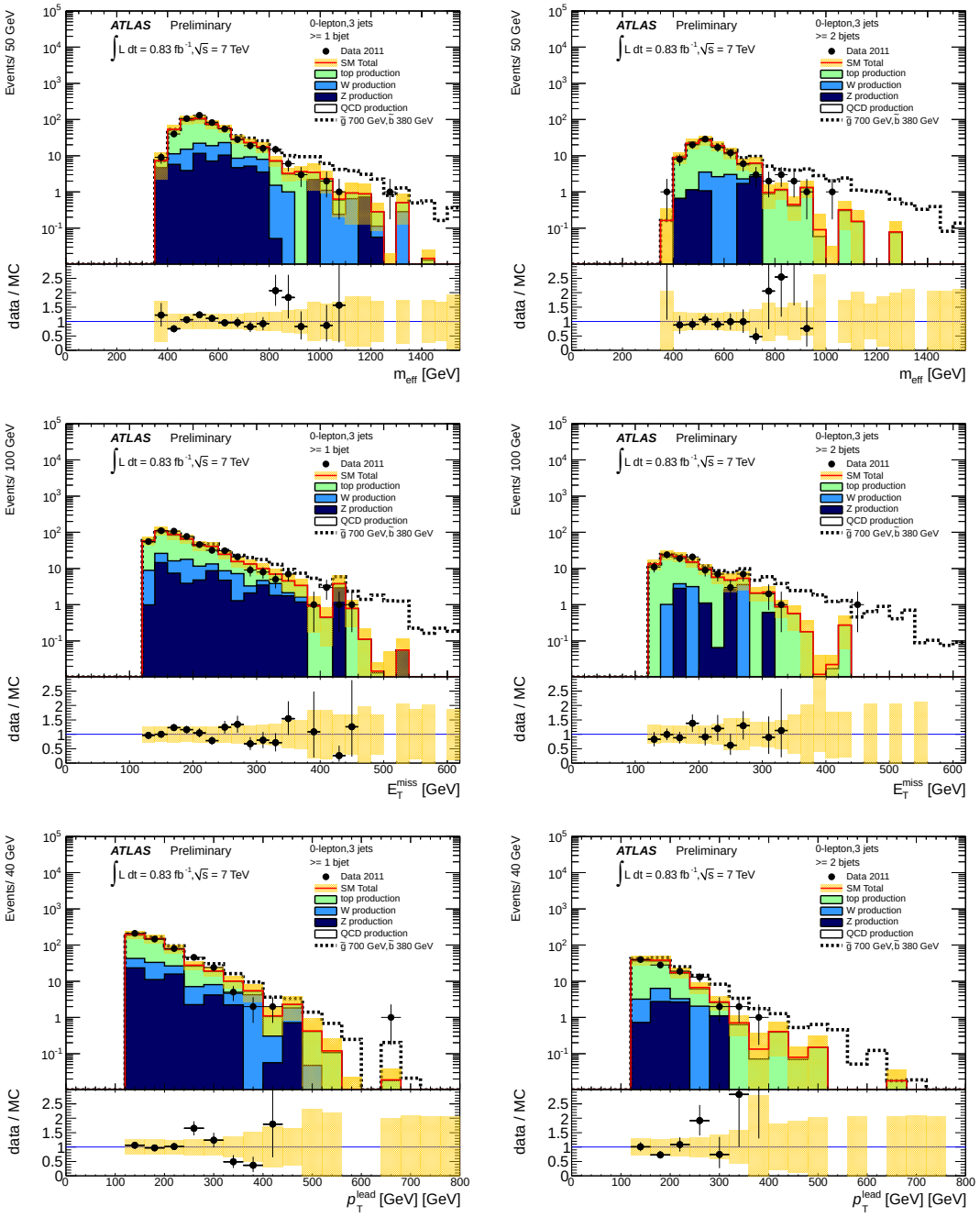

Figure 3: Distributions of the effective mass, m_{eff} (top), E_T^{miss} (middle) and the p_T of the leading jet (bottom) for data and the expected SM processes in the 1 *b*-tag (left) and 2 *b*-tags (right) signal regions. The yellow band shows the full systematic uncertainty on the SM expectation. For illustration, the distributions of one reference SUSY signal are superimposed. The lower plot shows the bin-by-bin ratio of the data to the SM expectation.

Sig. Reg.	Data (0.83 fb^{-1})	Top	W/Z	QCD	Total
3JA (1 btag m_{eff} >500 GeV)	361	221^{+82}_{-68}	121 ± 61	15 ± 7	356^{+103}_{-92}
3JB (1 btag m_{eff} >700 GeV)	63	37^{+15}_{-12}	31 ± 19	1.9 ± 0.9	70^{+24}_{-22}
3JC (2 btag m_{eff} >500 GeV)	76	55^{+25}_{-22}	20 ± 12	3.6 ± 1.8	79^{+28}_{-25}
3JD (2 btag m_{eff} >700 GeV)	12	$7.8^{+3.5}_{-2.9}$	5 ± 4	0.5 ± 0.3	$13.0^{+5.6}_{-5.2}$

Table 2: Summary observed and expected event yields in the four signal regions. The QCD prediction is based on the jet smearing method described in the text. Systematic uncertainties for the Standard Model predictions are given.

translated into 95% C.L. upper limits on contributions from new physics. Limits are derived using the CL_s [41] method, while the power constrained limit (PCL) [42] method is used for comparison with previous ATLAS results. Upper limits at 95% C.L. on the number of signal events are converted into model-independent 95% C.L. upper limits on the effective cross sections for new processes. The results in Table 3 show that the region 3JD provides the most stringent effective cross section upper limit of 17 fb.

Sig. Reg.	95% C.L. N events CL_s (PCL)	95% C.L. σ_{eff}(pb) CL_s (PCL)
3JA (1 btag m_{eff} >500 GeV)	240 (206)	0.288 (0.247)
3JB (1 btag m_{eff} >700 GeV)	51 (40)	0.061 (0.048)
3JC (2 btag m_{eff} >500 GeV)	65 (53)	0.078 (0.064)
3JD (2 btag m_{eff} >700 GeV)	14 (11)	0.017 (0.014)

Table 3: 95% C.L. upper limits on the non-SM contributions to the four signal regions. The corresponding PCL limits are given in parenthesis. Limits are given on the number of signal events and in terms of effective cross sections. The systematic uncertainties on the SM background estimation discussed in Section 5 are included.

The results are also interpreted in terms of 95% C.L. exclusion limits for several SUSY scenarios. In Figure 4 the observed and expected exclusion regions are shown in the $(m_{\tilde{g}}, m_{\tilde{b}_1})$ plane for the hypothesis that the lightest squark $\tilde{b}_1$ is produced via gluino-mediated or direct pair production and decays exclusively via $\tilde{b}_1 \to b\tilde{\chi}^0_1$. The NLO cross sections are calculated using `PROSPINO`. For each scenario, the signal region resulting in the best expected exclusion limit is used: the selection 3JD provides the best sensitivity in most cases. If $\Delta M(\tilde{g} - \tilde{b}_1) < 100$ GeV, signal regions with 1 b-tag are preferred, due to the lower number of expected b-jets above p_{T} thresholds. The regions 3JA and 3JB provide the best sensitivity when $m_{\tilde{g}} \gg m_{\tilde{b}_1}$ and sbottom pair production dominates. All systematic uncertainties on the signal and background contributions are taken into account in these limits and include the fully correlated detector-type uncertainties (JES, b-tagging, trigger, pile-up effects, luminosity) as well as the theoretical uncertainties on the signal (Renormalization/Factorization scale and PDF). Gluino masses below 720 GeV are excluded for sbottom masses up to 600 GeV. The exclusion is less stringent in the region with low $\Delta M(\tilde{g} - \tilde{b}_1)$, where low $E_{\text{T}}^{\text{miss}}$ is expected. This search extends the previous ATLAS exclusion limit in the same scenario by about 130 GeV (180 GeV if using the same limit setting procedure).

Results are also interpreted in the context of simplified models. In this case, all the squarks

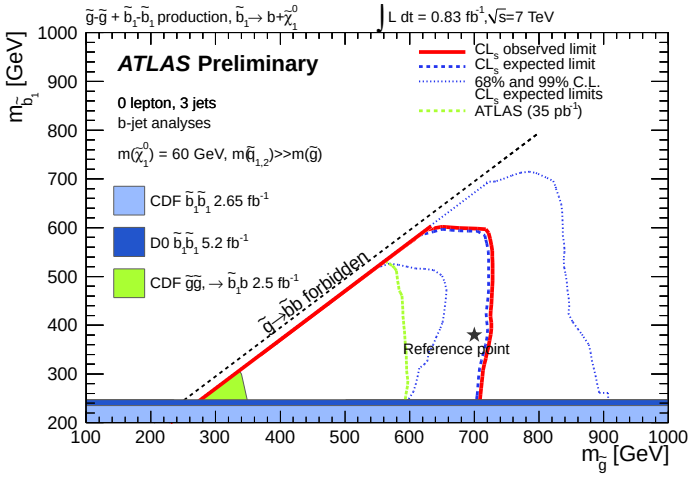

Figure 4: Observed and expected 95% C.L. exclusion limits in the $(m_{\tilde{g}}, m_{\tilde{b}_1})$ plane. Also shown are the 68% and 99% C.L. expected exclusion curves. For each point in the plot, the signal region selection providing the best expected limit is chosen. The neutralino mass is set to 60 GeV. The result is compared to previous results from ATLAS and CDF searches which assume the same gluino-sbottom decays hypotheses. Exclusion limits from the CDF and D0 experiments on direct sbottom pair production are also shown.

are heavier than the gluino, which decays exclusively into three-body final states ($b\bar{b}\tilde{\chi}_1^0$) via an off-shell sbottom. Such a scenario can be considered complementary to the previous one. The exclusion limits obtained on the $(m_{\tilde{g}}, m_{\tilde{\chi}_1^0})$ plane are shown in Figure 5 for gluino masses above 200 GeV. For each combination of masses, the analysis providing the best expected limit is chosen. The selection 3JD leads to the best sensitivity for gluino masses above 400 GeV and $\Delta M(\tilde{g} - \tilde{\chi}_1^0) > 100$ GeV. At low $\Delta M(\tilde{g} - \tilde{\chi}_1^0)$, soft b-jets spectra and low $E_{\mathrm{T}}^{\mathrm{miss}}$ are expected, giving higher sensitivity to the signal regions 3JA and 3JB are preferred. Low gluino mass scenarios present moderate m_{eff} and high b-jet multiplicity, thus favouring signal region 3JC. Neutralino masses below 200-250 GeV are excluded for gluino masses in the range 200-660 GeV, if $\Delta M(\tilde{g} - \tilde{\chi}_1^0)$ >100 GeV.

The results can be generalised in terms of 95% C.L. upper cross section limits for gluino-like pair production processes with produced particles decaying into $b\bar{b}\tilde{\chi}_1^0$ final states. The cross section upper limits versus the gluino and neutralino mass are also given in Figure 5.

The results are finally employed to extract limits on the gluino mass in the two SO(10) scenarios, DR3 and HS. Gluino masses below 570 GeV are excluded for the DR3 model. In this case $\tilde{g} \rightarrow b\bar{b}\tilde{\chi}_1^0$ decays dominate up to gluino masses of 550 GeV: above this range, high BR for different decay modes decrease the sensitivity of the selected final states. A lower sensitivity, $m_{\tilde{g}} < 450$ GeV, is found for the HS model, where larger branching ratios of $\tilde{g} \rightarrow b\bar{b}\tilde{\chi}_2^0$ are expected and the efficiency of the selection is reduced with respect to the DR3 case ($m_{\tilde{\chi}_2^0} \approx 2 \times m_{\tilde{\chi}_1^0}$).

7 Conclusions

An update on the search for supersymmetry in final states with missing transverse momentum, b-jet candidates and no isolated leptons in proton-proton collisions at 7 TeV is presented. The results are based on data corresponding to an integrated luminosity of 0.83 fb^{-1} collected

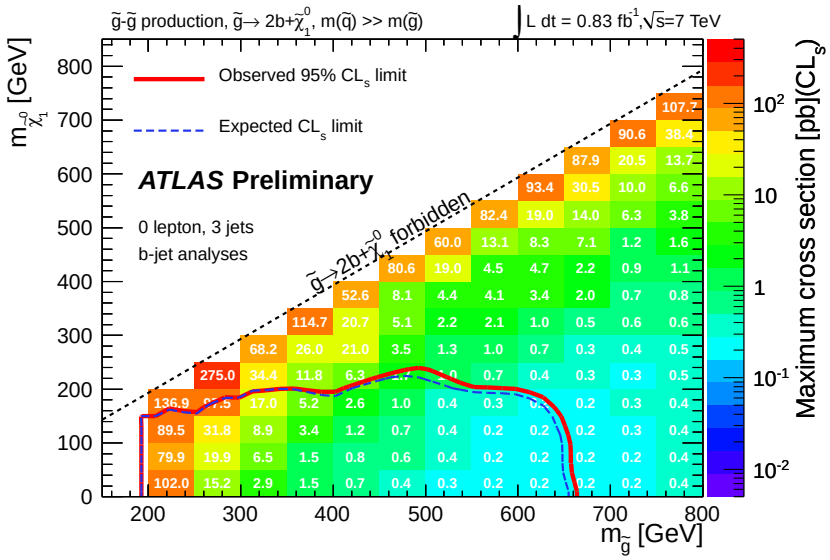

Figure 5: 95% C.L. upper cross section limits in pb and observed and expected limit contours in the $(m_{\tilde{g}}, m_{\tilde{\chi}_1^0})$ plane for gluino masses above 200 GeV. For each scenario, the signal region selection providing the best expected limit is chosen.

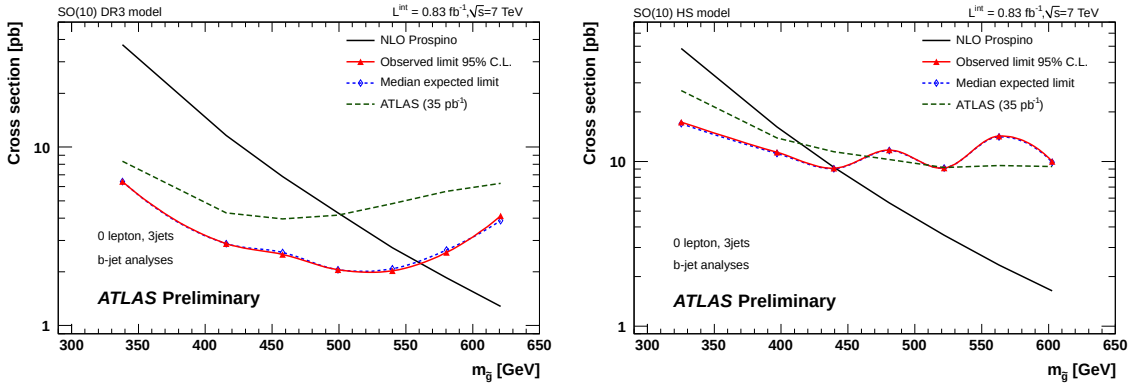

Figure 6: The observed and expected 95% C.L. limit on the production cross sections for the DR3 (*left*) and HS models (*right*) as a function of the gluino mass, as obtained using the selection which results in the best expected limit. The theoretical uncertainties on the NLO cross sections are included in the limit calculation.

during 2011 by the ATLAS experiment at the LHC. Events with at least three energetic jets, large $E_{\mathrm{T}}^{\mathrm{miss}}$ and at least one b-tagged jet are selected in four signal regions based on the number of b-tagged jets ($\geq$1 or $\geq$2 b-jets) and on the value of effective mass (>500 or >700 GeV). The dominant Standard Model backgrounds are estimated from Monte Carlo simulation and are validated with data.

No excess above the expectation from Standard Model processes is found. The results are used to exclude parameter regions in various R-parity conserving SUSY models. Under the assumption that the lightest squark $\tilde{b}_1$ is produced via gluino-mediated processes or direct pair production and decays exclusively via $\tilde{b}_1 \rightarrow b\tilde{\chi}_0$, gluino masses below 720 GeV are excluded with 95% C.L. for sbottom masses up to 600 GeV using the CL_s approach. This extends the pre-

vious (35 pb^{-1}) ATLAS limits on gluino masses in the same scenario by about 130 GeV. Results are also interpreted in simplified models, where gluinos decay into heavy flavour final states ($b\bar{b}\tilde{\chi}_1^0$) via an off-shell sbottom. In these scenarios exclusion limits in the ($m_{\tilde{g}}, m_{\tilde{\chi}_1^0}$) plane are derived and $\tilde{\chi}_1^0$ masses below 200-250 GeV are excluded for gluino masses below 660 GeV, if $\Delta M(\tilde{g} - \tilde{\chi}_1^0)$ >100 GeV. 95% C.L. upper cross section limits for gluino-like pair production processes with produced particles decaying into $b\bar{b}\tilde{\chi}_1^0$ final states are also given. Finally, in specific SUSY breaking models based on the gauge group SO(10), gluinos with masses below 570 GeV and 450 GeV are excluded for the DR3 and HS models, respectively, extending previously excluded ranges by about 50 and 30 GeV.

References

[1] Yu.A. Golfand and E.P. Likhtman, JETP Lett. **13** (1971) 323; A. Neveu and J.H. Schwartz, Nucl. Phys. **B31** (1971) 86; A. Neveu and J.H. Schwartz, Phys. Rev. **D4** (1971) 1109; P. Ramond, Phys. Rev. **D3** (1971) 2415; D.V. Volkov and V.P. Akulov, Phys. Lett. **B46** (1973) 109; J. Wess and B. Zumino, Phys. Lett. **B49** (1974) 52; J. Wess and B. Zumino, Nucl. Phys. **B70** (1974) 39; P. Fayet, Phys. Lett. **B69** (1977) 489; G.R. Farrar and P. Fayet, Phys. Lett. **B76** (1978) 575 .

[2] S. P. Martin, `arXiv:hep-ph/9709356 (1997)`.

[3] ATLAS Collaboration, Phys. Lett. **B701** (2011) 398–416.

[4] CMS Collaboration, `arXiv:1106.3272 [hep-ex] (2011)`.

[5] ATLAS Collaboration, JINST **3** (2008) S08003.

[6] D. e. a. Alves, `arXiv:1105.2838 [hep-ph] (2011)`.

[7] M. Gell-Mann, P. Ramond, and R. Slansky, Rev.Mod.Phys. **50** (1978) 721.

[8] H. Baer, S. Kraml, A. Lessa, and S. Sekmen, JHEP **1002** (2010) 055.

[9] G. Corcella et al., JHEP **01** (2001) 010.

[10] F. Paige, S. Protopopescu, H. Baer, and X. Tata, `arXiv:hep-ph/0312045 (2003)`.

[11] A. Djouadi, M. M. Muhlleitner, and M. Spira, Acta Phys. Polon. **B38** (2007) 635–644.

[12] W. Beenakker, R. Hopker, and M. Spira, `arXiv:hep-ph/9611232 (1996)`.

[13] D. Stump et al., JHEP **10** (2003) 046.

[14] R. Hamberg, W. L. van Neerven, and T. Matsuura, Nucl. Phys. **B359** (1991) 343–405. Erratum-ibid. B644:403-404,2002.

[15] K. Melnikov and F. Petriello, Phys. Rev. **D74** (2006) 114017.

[16] K. Melnikov and F. Petriello, Phys. Rev. Lett. **96** (2006) 231803.

[17] R. Bonciani, S. Catani, M. L. Mangano, and P. Nason, Nucl. Phys. **B529** (1998) 424–450.

[18] S. Moch and P. Uwer, Phys. Rev. **D78** (2008) 034003.

[19] M. Beneke, M. Czakon, P. Falgari, A. Mitov, and C. Schwinn, arXiv:0911.5166 [hep-ph] (2009).

[20] N. Kidonakis, Phys.Rev. **D83** (2011) 091503.

[21] N. Kidonakis, Phys.Rev. **D81** (2010) 054028.

[22] S. Frixione and B. Webber, arXiv:hep-ph/0601192 (2006).

[23] S. Frixione, P. Nason, and B. Webber, JHEP **08** (2003) 007.

[24] S.Frixione et al., JHEP **11** (2007) 070.

[25] M. Mangano et al., JHEP **07** (2003) 001.

[26] B. P. Kersevan and E. Richter-Was, arXiv:hep-ph/0405247 (2004).

[27] ATLAS Collaboration, ATLAS-CONF-2010-031 (2010).

[28] GEANT4 Collaboration, S. Agostinelli et al., Nucl. Instrum. Meth. **A506** (2003) 250–303.

[29] ATLAS Collaboration, Eur.Phys.J. **C70** (2010) 823–874.

[30] J. Butterworth, J. R. Forshaw, and M. Seymour, Z.Phys. **C72** (1996) 637–646.

[31] D. Casadei et al., ATL-DAQ-PUB-2011-001 (2011).

[32] M. Cacciari, G. P. Salam, and G. Soyez, JHEP **0804** (2008) 063.

[33] M. Cacciari and G. P. Salam, Physics Letters B **641** (2006) no. 1, 57 – 61.

[34] M. Cacciari, G. P. Salam, and G. Soyez, http://fastjet.fr/ .

[35] ATLAS Collaboration, ATLAS-CONF-2011-032 (2011).

[36] ATLAS Collaboration, ATLAS-CONF-2011-089 (2011).

[37] ATLAS Collaboration, ATL-PHYS-PUB-2011-006 (2011).

[38] ATLAS Collaboration, Phys. Lett. **B701** (2011) 186–203.

[39] ATLAS Collaboration, ATLAS-CONF-2011-086 (2011).

[40] ATLAS Collaboration, ATLAS-CONF-2011-011 (2011).

[41] A. L. Read, J. Phys. **G28** (2002) 2693–2704.

[42] G. Cowan, Eur. Phys. J. **C71** (2011) 1554.